NANO LETTERS

pubs.acs.org/NanoLett Letter

Anomalous Stopping and Charge Transfer in Proton-Irradiated Graphene

Alina Kononov and André Schleife*

Cite This: *Nano Lett.* 2021, 21, 4816–4822 Read Online

ACCESS | Metrics & More | Article Recommendations | Supporting Information

ABSTRACT: We use first-principles calculations to uncover and explain a new type of anomalous low-velocity stopping effect in proton-irradiated graphene. We attribute a shoulder feature that occurs exclusively for channeling protons to enhanced electron capture from σ- and π-orbitals. Our analysis of electron emission indicates that backward emission is more sensitive to proton trajectory than forward emission and could thus produce higher contrast images in ion microscopy. For slow protons, we observe a steep drop in emission, consistent with predictions from analytical models.

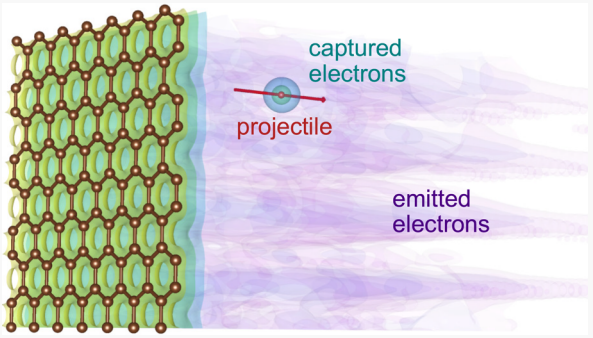

KEYWORDS: *graphene, time-dependent density functional theory, electronic stopping power, electron capture, electron emission*

Graphene, an exceptionally strong and intrinsically semimetallic sheet of carbon atoms arranged in a honeycomb lattice,[1−4] was the first 2D material ever fabricated[1] and remains promising as a conductive layer in novel electronics based on 2D heterostructures.[5] It has attracted enormous interest due to its potential for transistors,[1,6−8] solar cells,[9] detectors,[10,11] plasmonics,[12] qubits,[13] and other devices.[9,14] However, graphene's sensitivity to defects and nanostructural features, which can degrade performance when undesirable[15,16] or enable an application when intentional,[17−21] poses a major obstacle for scalable fabrication of graphene-based devices.

Consequently, precise techniques for characterization, patterning, and defect engineering of 2D materials including graphene are necessary to realize their incredible potential. Focused ion beams are promising in this context, with several empirical demonstrations of their capability to image[22,23] and characterize[24] 2D materials, create point defects in them[17,18,25] or otherwise alter their atomic structure,[19,20,26−31] and tune their mechanical[25] and electronic[29] properties. However, ion beam parameters must be specially tuned for 2D materials because they exhibit a highly pre-equilibrium response to ion irradiation which differs from bulk and thin films. Highly charged ions partially neutralize[32,33] and reach an equilibrium charge state only after traversing ∼10 nm of material,[34,35] leading to deviations from bulk behavior for atomically thin systems.[36] Even in the case of proton irradiation, surface plasmons are predicted to enhance energy deposition,[37] and the radically different plasmonic properties of 2D materials[38,39] should further influence charge and energy transfer processes upon ion impact.

Despite the practical importance of ion beam techniques, a detailed understanding of the unique physics occurring during an energetic ion's traversal of a 2D material remains elusive. While experimental work routinely identifies intriguing results of applying specific beam parameters to particular materials, direct observation of the underlying mechanisms is limited by spatial and temporal resolutions of measurement techniques. Accurate first-principles calculations offer a promising alternative, enabling extremely detailed simulations of femtosecond-scale dynamics after a single ion impact. Indeed, numerous studies[32,40−54] have demonstrated the predictive power of such calculations for bulk materials under ion irradiation, showing, for instance, that directional bonding in semiconductors and insulators makes electronic stopping sensitive to ion trajectory even for slow ions, when core electrons are negligible.[32,47,52,54]

Additionally, computational studies[48−53] have elucidated experimentally observed[55−57] threshold effects in low-velocity stopping power, where exciting electrons across a band gap requires a minimum projectile velocity. Similar effects can be expected for electron emission, where transferring sufficient energy for electrons to overcome the work function would require a minimum projectile velocity. Although experiments

Received: April 10, 2021
Revised: May 13, 2021
Published: May 25, 2021

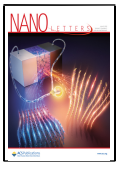

https://doi.org/10.1021/acs.nanolett.1c01416
Nano Lett. 2021, 21, 4816–4822

support their existence,[58,59] to date no first-principles study has examined such threshold emission effects. Furthermore, graphene presents a highly interesting case with directional bonding but no band gap. While previous work[60−67] has simulated ion-irradiated 2D materials, none has established the connection between energy transfer, charge capture, and electron emission, or even separately analyzed emissions from both sides of the material.

In this Letter, we present a comprehensive, first-principles computational study of proton-irradiated graphene and discover a new type of anomalous effect in energy deposition by slow ions with less than 1 atomic unit (at. u.) of velocity. This effect only occurs along some proton trajectories and is accompanied by enhanced electron capture by the projectile. Furthermore, calculations of emitted electron yields from both sides of the material lead to predictions relevant to ion beam microscopy and the first first-principles study of threshold electron emission.

We begin with a discussion of energy deposition for different proton impact points (see Figure 1a). While proton-irradiated graphene has been simulated before,[62−64] including some exploration of different impact points,[62,63] a comprehensive understanding of the trajectory dependence of energy deposition remains absent. Our analysis allows us to interpret the underlying physics in terms of spatial inhomogeneity of the electron density arising from chemical bonding in graphene. For the centroid impact point, which is often considered a good approximation to an ensemble average over all trajectories,[41,45,63] our results for energy transferred from proton to graphene agree well with earlier TDDFT calculations[63,64] and empirical data for per-layer electronic stopping power of hydrogen in graphite[68] (see Figure 1b). We discuss potential sources of minor discrepancies among computed energy transfer results in the Supporting Information (SI).

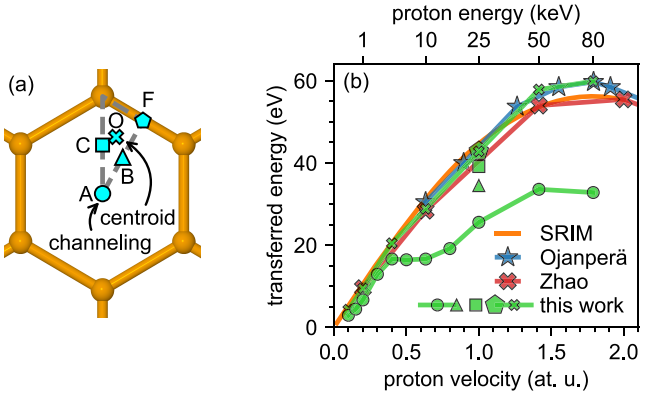

Figure 1. (a) Proton impact points (cyan) in monolayer graphene (orange) investigated here. The projectile always travels normal to the graphene plane. (b) Total energy deposited in graphene by energetic protons. Results from this work are compared to SRIM[68] and previous TDDFT results.[63,64] Symbols correspond to the different impact points illustrated in (a).

Interestingly, we find that energy transfer is quite sensitive to the impact point: We compute considerably lower electronic stopping for the channeling than for the centroid trajectory at velocities above 0.4 at. u. (see Figure 1b). This contrasts with behavior in bulk metals, where valence electrons are largely delocalized and stopping power depends strongly on the projectile's trajectory only for velocities sufficiently high to excite localized core electrons.[40,41] However, our finding confirms earlier reports of higher energy deposition when the proton passes through a C—C bond than through the center of the hexagon.[62,63] Trajectory-dependent stopping power has also been reported in bulk semiconductors such as Si,[32] Ge,[52] graphite,[54] and phosphide-based compounds.[47] In these materials, directional bonding leads to differences in the electron density with which the projectile interacts when moving along different channels, causing strong trajectory dependence of electronic stopping. Nonetheless, studies finding channel-dependent stopping in bulk materials largely observed the same qualitative behavior as a function of projectile velocity across different channels, namely, a featureless rise[52] toward a single peak[32,47] positioned near the experimental maximum even while the peak height depends on projectile trajectory. As a notable exception, graphite exhibits slightly different behavior for projectiles traveling at different angles with respect to the graphitic planes.[54]

Conversely, we found dramatically different behavior for different normal trajectories through graphene: energy transferred along a channeling trajectory in graphene exhibits an unusual, bimodal velocity dependence featuring a shoulder between 0.4 and 0.7 at. u. of velocity (see Figure 1). Similar features appeared in the results of Bubin et al. for proton-irradiated graphene fragments,[62] but no explanation was offered. Deviations from linear low-velocity stopping are typically attributed to band structure effects. In insulators[48−51,55,56] and semiconductors,[52,53,57] slow projectiles cannot excite electrons across the band gap, and in metals,[42−44,59,69−71] slow projectiles cannot excite electrons from deeper valence bands. However, to our knowledge no study has explained the anomalous trajectory dependence of stopping for semimetallic 2D graphene.

To explain this behavior, we examine both the electronic structure and the spatial distributions of partial electron densities of graphene in Figure 2. Our analysis reveals that high-energy states lying less than 2.75 eV below the valence band maximum (VBM), commonly known as π-electrons, are more localized in-plane around the carbon atoms than lower-

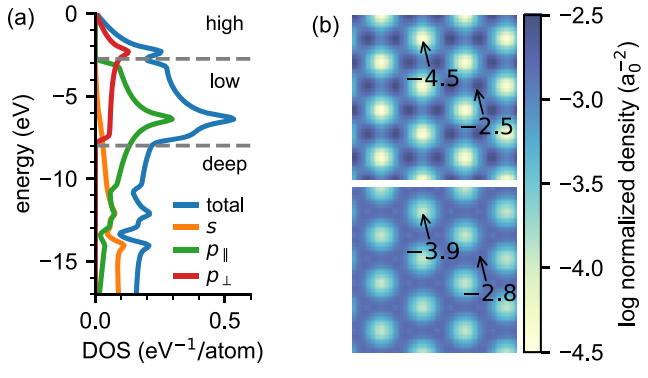

Figure 2. (a) Projected density of states of ground-state graphene with valence band divisions indicated by horizontal dashed lines (see text). Energies are referenced to the valence band maximum. (b) Ground-state electron density contributed by the high-energy (top) and low-energy (bottom) graphene valence bands. Electron density has been integrated along the direction normal to graphene and is normalized by the number of electrons within each set of bands. Annotations indicate minimum and maximum values.

https://doi.org/10.1021/acs.nanolett.1c01416
Nano Lett. 2021, 21, 4816−4822

energy states (between 2.75 and 8 eV below the VBM), consisting of both π- and σ-orbitals. This spatial inhomogenity and spectral separation suggests that high-energy states could be more difficult for a channeling proton to excite, and below we explore how these observations affect velocity-dependent stopping.

Specifically, to investigate the source of the shoulder-like feature in the stopping power of channeling protons, we examined the occupation of the original, ground-state orbitals after irradiation and the extent to which the proton excites electrons from different bands. We obtained the excited electron contribution $n_j(t)$ from a ground-state KS orbital $|\phi_j^{(GS)}\rangle$ by summing over projections of the time-dependent KS orbitals $|\phi_l(t)\rangle$,

$$n_j(t) = 2\left(1 - \sum_l \left|\left\langle \phi_l(t)|\phi_j^{(GS)}\right\rangle\right|^2\right) \quad (1)$$

where the factor of 2 accounts for spin degeneracy. Subsequently, the $n_j(t)$ were summed over states within the particular energy bands illustrated in Figure 2a; the results become constant over time (see Figure S1 in the SI), and we report the number of electrons excited from each band at the end of each simulation in Figure 3.

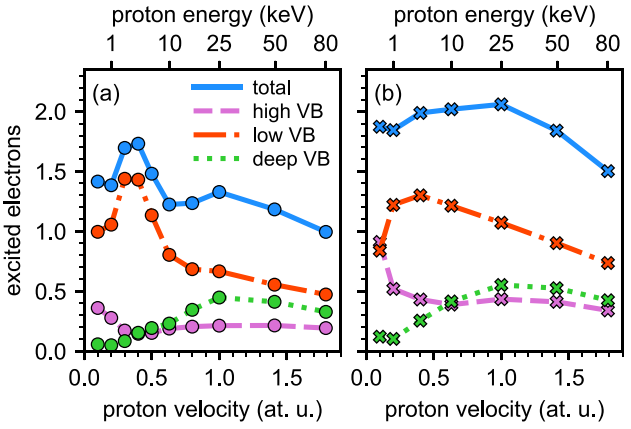

Figure 3. Number of electrons excited after a proton traverses graphene (a) along the channeling trajectory and (b) along the centroid trajectory. The total number of excited electrons is decomposed into contributions from the different sets of valence bands illustrated in Figure 2a.

Figure 3 shows that the shoulder in the energy transfer for channeling protons is associated with a drop in the total number of electrons excited. Analysis of the contributions of different valence bands provides deeper insight. While a channeling proton indeed excites high-energy valence electrons at lower rates than a proton traversing the centroid trajectory (as suggested by the electron density distributions in Figure 2b), this effect remains nearly constant throughout the entire velocity range. Unexpectedly, the most striking difference between the excitations induced along different proton trajectories occurs in the low-energy valence bands, where the number of electrons excited by the channeling proton exhibits a much more pronounced maximum near velocities of 0.3−0.4 at. u. We thus conclude that the features in the total number of excited electrons and in electronic stopping near those velocities mainly originate from the low-energy valence bands. Finally, the extent of deep valence band excitation is not sensitive to projectile trajectory in this velocity range.

Analyzing the charge captured by the projectile after transmission through graphene offers additional insight into the physics of trajectory-dependent stopping. For the centroid trajectory, our results for electron capture agree well with previous calculations[64] and show the same trend of decreasing capture for faster protons (see Figure 4) reported for proton-

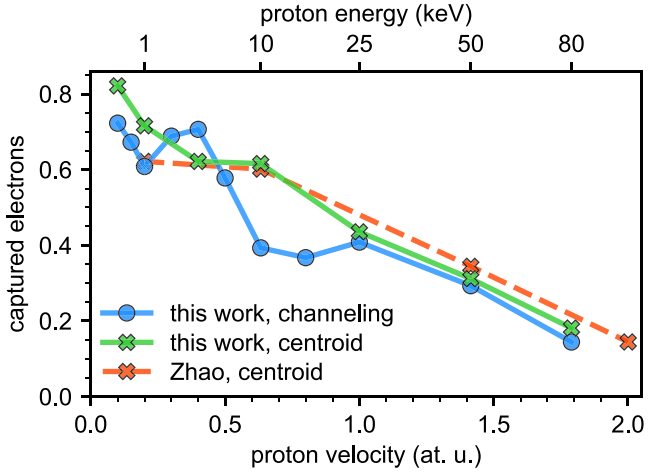

Figure 4. Electrons captured by the proton after transmission through graphene along channeling and centroid trajectories. Results from this work are compared to previous TDDFT results.[64]

irradiated aluminum.[37] However, for channeling protons, the enhanced excitation at velocities of 0.3−0.4 at. u. (see Figure 3) is accompanied by a similar feature in the number of electrons captured by the projectile (see Figure 4). This suggests that resonant electron capture from the low-energy valence bands may be responsible for the shoulder in energy transfer for channeling protons. Experiments such as those in ref 36, which simultaneously measure projectile energy loss and charge state, could potentially confirm this prediction.

While our above analysis of energy deposition can help explain eventual radiation damage, ion-induced electron emission has additional implications for imaging.[22,23,72−74] Here, we calculate emitted electron yields for the side from which the projectile approaches before impact (entrance-side) and the side from which it emerges (exit-side). Interestingly, the exit-side and entrance-side emissions shown in Figure 5 exhibit very different velocity dependencies; maximum entrance-side emission occurs at a velocity of 0.63 at. u., while the peak in exit-side emission occurs much closer to the stopping maximum at a velocity of 1.41 at. u. Furthermore, the exit-side emission is more sensitive to proton trajectory, particularly near the emission maximum, where the centroid trajectory yields 65% more electrons than the channeling trajectory. These findings indicate that detecting exit-side electron emission after irradiation by 50 keV protons may provide high contrast images of graphene samples, especially since protons at this energy are not expected to damage the atomic structure.[62]

Finally, our first-principles results also describe behavior near the theoretically expected but experimentally elusive kinetic emission threshold for slow projectiles. We observe a steep drop in electron emission with less than 0.02 electrons emitted for a proton with 0.1 at. u. of velocity (see Figure 5).

https://doi.org/10.1021/acs.nanolett.1c01416
Nano Lett. 2021, 21, 4816−4822

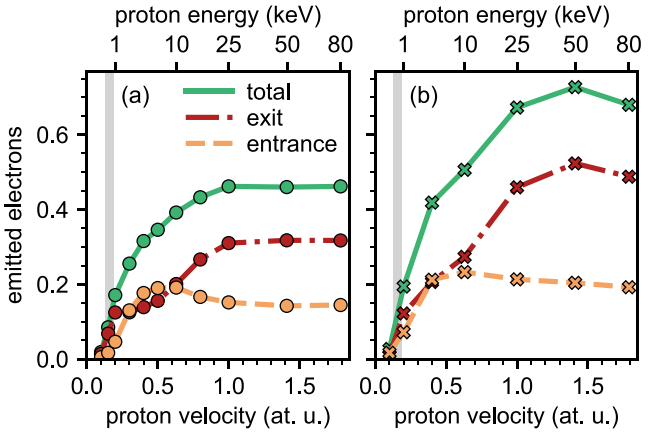

Figure 5. Electrons emitted after a proton traverses graphene along the (a) channeling and (b) centroid trajectory. The total number of emitted electrons is decomposed into exit-side and entrance-side emission. The gray bar indicates the range of threshold velocities predicted by different analytic models.

This is consistent with the threshold velocities v_{th} = 0.13−0.19 at. u. predicted by several analytic models[43,53,58,75] (see details in eqs S1−S3 of the SI). However, these estimates for v_{th} can be understood to predict the velocity below which the projectile cannot excite electrons directly into the continuum, though it could still, for instance, excite electrons into conduction bands and subsequently promote them into the continuum. Thus, the low but nonzero emitted electron yields that we calculate for a proton velocity of 0.1 at. u. may represent nonlinear or subthreshold emission, which has been indirectly measured.[76]

We note that in addition to such subthreshold effects, numerical uncertainties also limit the conclusiveness of our emission predictions for proton velocities below 0.2 at. u. This includes the sensitivity of low emission data to the precise definition of the material-vacuum boundary, since accurately distinguishing emitted electrons with extremely low kinetic energy from an excess electron density on the graphene surface would require very long simulation times. The time needed for an electron with kinetic energy E to emerge into the vacuum scales inversely with its velocity or as $1/\sqrt{E}$. We do not expect recapturing of electrons by graphene to introduce uncertainties, since this process does not occur during our few-femtosecond simulations (see Figure S2 of the SI) and the positive charge induced in the graphene spreads out too quickly to attract escaping electrons strongly.

In summary, we found an anomaly in low-velocity energy deposition by channeling protons in graphene which does not occur for protons traversing a centroid trajectory. This behavior is accompanied by pronounced features in the numbers of electrons excited from lower-energy graphene valence states and those captured by the proton. Thus, we propose that this anomalous behavior is caused by resonant projectile charge capture from the lower-energy valence bands. Since a projectile's charge equilibrates after traversing a few nanometers of material, this effect may be specific to few-layer materials.

We also characterized electron emission from proton-irradiated graphene and found that exit-side emission is more sensitive to proton trajectory than entrance-side emission, making it a strong candidate for high-contrast imaging techniques. A steep drop in emitted electron yields for slow protons is consistent with threshold velocities predicted by analytical models. The quantitative predictions of our first-principles results open a new avenue for optimizing parameters for ion beam techniques and studying the fundamental physics of threshold emission effects in real materials.

METHODS

We performed real-time time-dependent density functional theory (TDDFT)[77−81] simulations of the excited electron dynamics in proton-irradiated monolayer graphene using the Qbox/Qb@ll code.[82−86] Converged ground-state single-particle Kohn−Sham (KS) states from DFT[87] served as the initial condition for real-time propagation of the time-dependent KS equations

$$i\frac{\partial}{\partial t}\phi_j(\mathbf{r}, t) = \left(-\frac{\nabla^2}{2} + V_{KS}[n](\mathbf{r}, t)\right)\phi_j(\mathbf{r}, t) \tag{2}$$

Here, ϕ_j are single-particle KS orbitals evolving in a time-dependent effective potential V_{KS} which is a functional of the electron density

$$n(\mathbf{r}, t) = \sum_j f_j \left|\phi_j(\mathbf{r}, t)\right|^2 \tag{3}$$

and f_j are orbital occupations.

KS states are represented in a plane-wave basis with a cutoff energy of 100 Ry, exchange and correlation (XC) is treated with the adiabatic local density approximation,[88,89] and the electron−ion interaction is described using HSCV pseudopotentials.[90] Atomic forces on all carbon atoms in the initial structure were relaxed to less than 2 meV/Å. Large simulation cells with 112 carbon atoms and 150 a_0 of vacuum were needed to converge electron emission, allowing reciprocal-space sampling using only the Γ-point. We address convergence with respect to cutoff energy and vacuum size in Figures S3 and S4 of the SI. To help interpret our TDDFT results, a projected density of states (DOS) for ground-state graphene was calculated using VASP[91,92] with a 4-atom supercell, 64 × 64 × 1 Γ-centered Monkhorst−Pack[93] **k** point mesh, and the same vacuum length, cutoff energy, and XC approximation as above; the obtained DOS is similar to previously reported results.[94−96]

We begin real-time propagation with the proton 25 a_0 away from the graphene. It then approaches and traverses the material at a constant velocity along a normal trajectory (see Figure 1a). Carbon nuclei are held fixed because the few-femtosecond time-scale of the simulations is too short for them to move appreciably. For numerical integration of the time-dependent KS equations, we use the enforced time reversal symmetry (ETRS) method[85,97] with a time step of 1.0 attosecond, a choice shown to evolve similarly large systems with exceptional accuracy.[37,98] For the case of a channeling proton impacting graphene with 1 at. u. of velocity, we found that using a time step half as large changed the charge and energy transfer by less than 0.1%.

The Hellmann−Feynman force on the projectile gives the instantaneous electronic stopping power, or rate of energy transfer from the proton to the material. To obtain the total energy transferred, the instantaneous stopping data (see Figure S6 in the SI) is integrated over a layer thickness taken as the interlayer separation in graphite, though we find very similar

https://doi.org/10.1021/acs.nanolett.1c01416
Nano Lett. 2021, 21, 4816−4822

trends for other possible choices such as the dielectric thickness reported in ref 99 (see Figure S7 in the SI).

Upon proton impact, electrons are emitted from both sides of the graphene. Entrance- and exit-side emitted electron yields are determined by integrating the time-dependent electron density from the TDDFT simulations over the corresponding vacuum regions (see details in Figure S5 of the SI) and subtracting electrons captured by the projectile, as determined by fits to analytical orbitals as described in ref 37. All inputs and outputs from our simulations are available at the Materials Data Facility.[100,101]

■ ASSOCIATED CONTENT

Supporting Information

The Supporting Information is available free of charge at https://pubs.acs.org/doi/10.1021/acs.nanolett.1c01416.

Supplemental discussion of small differences among computed stopping powers; time dependence of excited electron contributions, electron emission, and instantaneous stopping power; threshold emission models; convergence with respect to cutoff energy and vacuum length; integration boundaries for calculating emitted electron yields and insensitivity of energy transfer to definition of graphene thickness (PDF)

■ AUTHOR INFORMATION

Corresponding Author

André Schleife − *Department of Materials Science and Engineering, Materials Research Laboratory, and National Center for Supercomputing Applications, University of Illinois at Urbana−Champaign, Urbana, Illinois 61801, United States;* orcid.org/0000-0003-0496-8214; Email: schleife@illinois.edu

Author

Alina Kononov − *Department of Physics, University of Illinois at Urbana−Champaign, Urbana, Illinois 61801, United States;* orcid.org/0000-0002-6600-224X

Complete contact information is available at: https://pubs.acs.org/10.1021/acs.nanolett.1c01416

Notes

The authors declare no competing financial interest.

■ ACKNOWLEDGMENTS

We thank Pinshane Huang for stimulating discussions. This material is based upon work supported by the National Science Foundation under Grant OAC-1740219. Support from the IAEA F11020 CRP "Ion Beam Induced Spatiotemporal Structural Evolution of Materials: Accelerators for a New Technology Era" is gratefully acknowledged. This research is part of the Blue Waters sustained-petascale computing project, which is supported by the National Science Foundation (awards OCI-0725070 and ACI-1238993) and the state of Illinois. Blue Waters is a joint effort of the University of Illinois at Urbana−Champaign and its National Center for Supercomputing Applications. This work made use of the Illinois Campus Cluster, a computing resource that is operated by the Illinois Campus Cluster Program (ICCP) in conjunction with the National Center for Supercomputing Applications (NCSA) and which is supported by funds from the University of Illinois at Urbana−Champaign.

■ REFERENCES

(1) Novoselov, K. S. Electric Field Effect in Atomically Thin Carbon Films. *Science* **2004**, *306*, 666−669.

(2) Novoselov, K. S.; Geim, A. K.; Morozov, S. V.; Jiang, D.; Katsnelson, M. I.; Grigorieva, I. V.; Dubonos, S. V.; Firsov, A. A. Two-dimensional gas of massless Dirac fermions in graphene. *Nature* **2005**, *438*, 197−200.

(3) Geim, A. K.; Novoselov, K. S. The rise of graphene. *Nat. Mater.* **2007**, *6*, 183−191.

(4) Castro Neto, A. H.; Guinea, F.; Peres, N. M. R.; Novoselov, K. S.; Geim, A. K. The electronic properties of graphene. *Rev. Mod. Phys.* **2009**, *81*, 109−162.

(5) Geim, A. K.; Grigorieva, I. V. Van der Waals heterostructures. *Nature* **2013**, *499*, 419−425.

(6) Lin, Y.-M.; Jenkins, K. A.; Valdes-Garcia, A.; Small, J. P.; Farmer, D. B.; Avouris, P. Operation of Graphene Transistors at Gigahertz Frequencies. *Nano Lett.* **2009**, *9*, 422−426.

(7) Schwierz, F. Graphene transistors. *Nat. Nanotechnol.* **2010**, *5*, 487−496.

(8) Bertolazzi, S.; Krasnozhon, D.; Kis, A. Nonvolatile Memory Cells Based on MoS2/Graphene Heterostructures. *ACS Nano* **2013**, *7*, 3246−3252.

(9) Sun, Y.; Wu, Q.; Shi, G. Graphene based new energy materials. *Energy Environ. Sci.* **2011**, *4*, 1113−1132.

(10) Allegrini, F.; Ebert, R. W.; Fuselier, S. A.; Nicolaou, G.; Bedworth, P. V.; Sinton, S. W.; Trattner, K. J. Charge state of ∼ 1 to 50 keV ions after passing through graphene and ultrathin carbon foils. *Opt. Eng.* **2014**, *53*, 024101.

(11) Skoblin, G.; Sun, J.; Yurgens, A. Graphene bolometer with thermoelectric readout and capacitive coupling to an antenna. *Appl. Phys. Lett.* **2018**, *112*, 063501.

(12) Grigorenko, A. N.; Polini, M.; Novoselov, K. S. Graphene plasmonics. *Nat. Photonics* **2012**, *6*, 749−758.

(13) Wang, J. I.-J.; et al. Coherent control of a hybrid superconducting circuit made with graphene-based van der Waals heterostructures. *Nat. Nanotechnol.* **2019**, *14*, 120−125.

(14) Surwade, S. P.; Smirnov, S. N.; Vlassiouk, I. V.; Unocic, R. R.; Veith, G. M.; Dai, S.; Mahurin, S. M. Water desalination using nanoporous single-layer graphene. *Nat. Nanotechnol.* **2015**, *10*, 459−464.

(15) Tapasztó, L.; Dobrik, G.; Nemes-Incze, P.; Vertesy, G.; Lambin, P.; Biró, L. P. Tuning the electronic structure of graphene by ion irradiation. *Phys. Rev. B: Condens. Matter Mater. Phys.* **2008**, *78*, 233407.

(16) Vicarelli, L.; Heerema, S. J.; Dekker, C.; Zandbergen, H. W. Controlling Defects in Graphene for Optimizing the Electrical Properties of Graphene Nanodevices. *ACS Nano* **2015**, *9*, 3428−3435.

(17) Zhao, W.; Höfert, O.; Gotterbarm, K.; Zhu, J.; Papp, C.; Steinrück, H.-P. Production of Nitrogen-Doped Graphene by Low-Energy Nitrogen Implantation. *J. Phys. Chem. C* **2012**, *116*, 5062−5066.

(18) Bangert, U.; Pierce, W.; Kepaptsoglou, D. M.; Ramasse, Q.; Zan, R.; Gass, M. H.; Van den Berg, J. A.; Boothroyd, C. B.; Amani, J.; Hofsäss, H. Ion Implantation of Grapheneoward IC Compatible Technologies. *Nano Lett.* **2013**, *13*, 4902−4907.

(19) Bell, D. C.; Lemme, M. C.; Stern, L. A.; Williams, J. R.; Marcus, C. M. Precision cutting and patterning of graphene with helium ions. *Nanotechnology* **2009**, *20*, 455301.

(20) Kotakoski, J.; Brand, C.; Lilach, Y.; Cheshnovsky, O.; Mangler, C.; Arndt, M.; Meyer, J. C. Toward Two-Dimensional All-Carbon Heterostructures via Ion Beam Patterning of Single-Layer Graphene. *Nano Lett.* **2015**, *15*, 5944−5949.

(21) Li, Z.; Chen, F. Ion beam modification of two-dimensional materials: Characterization, properties, and applications. *Appl. Phys. Rev.* **2017**, *4*, 011103.

(22) Fox, D.; Zhou, Y. B.; O'Neill, A.; Kumar, S.; Wang, J. J.; Coleman, J. N.; Duesberg, G. S.; Donegan, J. F.; Zhang, H. Z. Helium ion microscopy of graphene: beam damage, image quality and edge contrast. *Nanotechnology* **2013**, *24*, 335702.

(23) Zhou, Y.; O'Connell, R.; Maguire, P.; Zhang, H. High throughput secondary electron imaging of organic residues on a graphene surface. *Sci. Rep.* **2015**, *4*, 7032.
(24) Guo, H.; Gao, J.; Ishida, N.; Xu, M.; Fujita, D. Characterization of two-dimensional hexagonal boron nitride using scanning electron and scanning helium ion microscopy. *Appl. Phys. Lett.* **2014**, *104*, 031607.
(25) Iberi, V.; Liang, L.; Ievlev, A. V.; Stanford, M. G.; Lin, M.-W.; Li, X.; Mahjouri-Samani, M.; Jesse, S.; Sumpter, B. G.; Kalinin, S. V.; Joy, D. C.; Xiao, K.; Belianinov, A.; Ovchinnikova, O. S. Nanoforging Single Layer $MoSe_2$ Through Defect Engineering with Focused Helium Ion Beams. *Sci. Rep.* **2016**, *6*, 30481.
(26) Ritter, R.; Wilhelm, R. A.; Stöger-Pollach, M.; Heller, R.; Mücklich, A.; Werner, U.; Vieker, H.; Beyer, A.; Facsko, S.; Gölzhäuser, A.; Aumayr, F. Fabrication of nanopores in 1 nm thick carbon nanomembranes with slow highly charged ions. *Appl. Phys. Lett.* **2013**, *102*, 063112.
(27) Hemamouche, A.; et al. FIB patterning of dielectric, metallized and graphene membranes: A comparative study. *Microelectron. Eng.* **2014**, *121*, 87−91.
(28) Wilhelm, R. A; Gruber, E.; Ritter, R.; Heller, R.; Beyer, A.; Turchanin, A.; Klingner, N.; Hubner, R.; Stoger-Pollach, M.; Vieker, H.; Hlawacek, G.; Golzhauser, A.; Facsko, S.; Aumayr, F. Threshold and efficiency for perforation of 1 nm thick carbon nanomembranes with slow highly charged ions. *2D Mater.* **2015**, *2*, 035009.
(29) Fox, D. S.; et al. Nanopatterning and Electrical Tuning of MoS2 Layers with a Subnanometer Helium Ion Beam. *Nano Lett.* **2015**, *15*, 5307−5313.
(30) Iberi, V.; Vlassiouk, I.; Zhang, X.-G.; Matola, B.; Linn, A.; Joy, D. C.; Rondinone, A. J. Maskless Lithography and in situ Visualization of Conductivity of Graphene using Helium Ion Microscopy. *Sci. Rep.* **2015**, *5*, 11952.
(31) Naitou, Y.; Iijima, T.; Ogawa, S. Direct nano-patterning of graphene with helium ion beams. *Appl. Phys. Lett.* **2015**, *106*, 033103.
(32) Lee, C.-W.; Stewart, J. A.; Dingreville, R.; Foiles, S. M.; Schleife, A. Multiscale simulations of electron and ion dynamics in self-irradiated silicon. *Phys. Rev. B: Condens. Matter Mater. Phys.* **2020**, *102*, 024107.
(33) Wilhelm, R. A.; Gruber, E.; Schwestka, J.; Heller, R.; Fascko, S.; Aumayr, F. Neutralization Dynamics of Slow Highly Charged Ions in 2D Materials. *Appl. Sci.* **2018**, *8*, 1050.
(34) Schenkel, T.; Briere, M. A.; Schmidt-Böcking, H.; Bethge, K.; Schneider, D. H. Electronic Sputtering of Thin Conductors by Neutralization of Slow Highly Charged Ions. *Phys. Rev. Lett.* **1997**, *78*, 2481−2484.
(35) Hattass, M.; Schenkel, T.; Hamza, A. V.; Barnes, A. V.; Newman, M. W.; McDonald, J. W.; Niedermayr, T. R.; Machicoane, G. A.; Schneider, D. H. Charge Equilibration Time of Slow, Highly Charged Ions in Solids. *Phys. Rev. Lett.* **1999**, *82*, 4795−4798.
(36) Wilhelm, R. A.; Gruber, E.; Ritter, R.; Heller, R.; Facsko, S.; Aumayr, F. Charge Exchange and Energy Loss of Slow Highly Charged Ions in 1 nm Thick Carbon Nanomembranes. *Phys. Rev. Lett.* **2014**, *112*, 153201.
(37) Kononov, A.; Schleife, A. Pre-equilibrium stopping and charge capture in proton-irradiated aluminum sheets. *Phys. Rev. B: Condens. Matter Mater. Phys.* **2020**, *102*, 165401.
(38) Eberlein, T.; Bangert, U.; Nair, R. R.; Jones, R.; Gass, M.; Bleloch, A. L.; Novoselov, K. S.; Geim, A.; Briddon, P. R. Plasmon spectroscopy of free-standing graphene films. *Phys. Rev. B: Condens. Matter Mater. Phys.* **2008**, *77*, 233406.
(39) Kinyanjui, M. K.; Kramberger, C.; Pichler, T.; Meyer, J. C.; Wachsmuth, P.; Benner, G.; Kaiser, U. Direct probe of linearly dispersing 2D interband plasmons in a free-standing graphene monolayer. *Europhys. Lett.* **2012**, *97*, 57005.
(40) Schleife, A.; Kanai, Y.; Correa, A. A. Accurate atomistic first-principles calculations of electronic stopping. *Phys. Rev. B: Condens. Matter Mater. Phys.* **2015**, *91*, 014306.
(41) Maliyov, I.; Crocombette, J.-P.; Bruneval, F. Electronic stopping power from time-dependent density-functional theory in Gaussian basis. *Eur. Phys. J. B* **2018**, *91*, 172.
(42) Zeb, M. A.; Kohanoff, J.; Sánchez-Portal, D.; Arnau, A.; Juaristi, J. I.; Artacho, E. Electronic Stopping Power in Gold: The Role of d Electrons and the H/He Anomaly. *Phys. Rev. Lett.* **2012**, *108*, 225504.
(43) Quashie, E. E.; Saha, B. C.; Correa, A. A. Electronic band structure effects in the stopping of protons in copper. *Phys. Rev. B: Condens. Matter Mater. Phys.* **2016**, *94*, 155403.
(44) Quashie, E. E.; Correa, A. A. Electronic stopping power of protons and alpha particles in nickel. *Phys. Rev. B: Condens. Matter Mater. Phys.* **2018**, *98*, 235122.
(45) Yost, D. C.; Kanai, Y. Electronic stopping for protons and α particles from first-principles electron dynamics: The case of silicon carbide. *Phys. Rev. B: Condens. Matter Mater. Phys.* **2016**, *94*, 115107.
(46) Yost, D. C.; Yao, Y.; Kanai, Y. Examining real-time time-dependent density functional theory nonequilibrium simulations for the calculation of electronic stopping power. *Phys. Rev. B: Condens. Matter Mater. Phys.* **2017**, *96*, 115134.
(47) Lee, C.-W.; Schleife, A. Electronic stopping and proton dynamics in InP, GaP, and $In_{0.5}Ga_{0.5}P$ from first principles. *Eur. Phys. J. B* **2018**, *91*, 222.
(48) Pruneda, J. M.; Sánchez-Portal, D.; Arnau, A.; Juaristi, J. I.; Artacho, E. Electronic Stopping Power in LiF from First Principles. *Phys. Rev. Lett.* **2007**, *99*, 235501.
(49) Zeb, M. A.; Kohanoff, J.; Sánchez-Portal, D.; Artacho, E. Electronic stopping power of H and He in Al and LiF from first principles. *Nucl. Instrum. Methods Phys. Res., Sect. B* **2013**, *303*, 59−61.
(50) Mao, F.; Zhang, C.; Dai, J.; Zhang, F.-S. First-principles study of the threshold effect in the electronic stopping power of LiF and SiO_2 for low-velocity protons and helium ions. *Phys. Rev. A: At., Mol., Opt. Phys.* **2014**, *89*, 022707.
(51) Li, C.-K.; Wang, F.; Liao, B.; OuYang, X.-P.; Zhang, F.-S. Ab initio electronic stopping power and threshold effect of channeled slow light ions in HfO_2. *Phys. Rev. B: Condens. Matter Mater. Phys.* **2017**, *96*, 094301.
(52) Ullah, R.; Corsetti, F.; Sánchez-Portal, D.; Artacho, E. Electronic stopping power in a narrow band gap semiconductor from first principles. *Phys. Rev. B: Condens. Matter Mater. Phys.* **2015**, *91*, 125203.
(53) Lim, A.; Foulkes, W.; Horsfield, A.; Mason, D.; Schleife, A.; Draeger, E.; Correa, A. Electron Elevator: Excitations across the Band Gap via a Dynamical Gap State. *Phys. Rev. Lett.* **2016**, *116*, 043201.
(54) Halliday, J.; Artacho, E. Anisotropy of electronic stopping power in graphite. *Phys. Rev. B: Condens. Matter Mater. Phys.* **2019**, *100*, 104112.
(55) Serkovic, L. N.; Sánchez, E. A.; Grizzi, O.; Eckardt, J. C.; Lantschner, G. H.; Arista, N. R. Stopping power of fluorides for low-velocity protons. *Phys. Rev. A: At., Mol., Opt. Phys.* **2007**, *76*, 040901.
(56) Markin, S. N.; Primetzhofer, D.; Bauer, P. Vanishing Electronic Energy Loss of Very Slow Light Ions in Insulators with Large Band Gaps. *Phys. Rev. Lett.* **2009**, *103*, 113201.
(57) Roth, D.; Goebl, D.; Primetzhofer, D.; Bauer, P. A procedure to determine electronic energy loss from relative measurements with TOF-LEIS. *Nucl. Instrum. Methods Phys. Res., Sect. B* **2013**, *317*, 61−65.
(58) Baragiola, R. A.; Alonso, E. V.; Oliva Florio, A. Electron emission from clean metal surfaces induced by low-energy light ions. *Phys. Rev. B: Condens. Matter Mater. Phys.* **1979**, *19*, 121−129.
(59) Markin, S. N.; Primetzhofer, D.; Prusa, S.; Brunmayr, M.; Kowarik, G.; Aumayr, F.; Bauer, P. Electronic interaction of very slow light ions in Au: Electronic stopping and electron emission. *Phys. Rev. B: Condens. Matter Mater. Phys.* **2008**, *78*, 195122.
(60) Miyamoto, Y.; Zhang, H. Electronic excitation in an Ar^{7+} ion traversing a graphene sheet: Molecular dynamics simulations. *Phys. Rev. B: Condens. Matter Mater. Phys.* **2008**, *77*, 161402.
(61) Zhang, H.; Miyamoto, Y.; Rubio, A. Ab initio Simulation of Helium-Ion Microscopy Images: The Case of Suspended Graphene. *Phys. Rev. Lett.* **2012**, *109*, 265505.

https://doi.org/10.1021/acs.nanolett.1c01416
Nano Lett. 2021, 21, 4816−4822

(62) Bubin, S.; Wang, B.; Pantelides, S.; Varga, K. Simulation of high-energy ion collisions with graphene fragments. *Phys. Rev. B: Condens. Matter Mater. Phys.* **2012**, *85*, 235435.
(63) Ojanperä, A.; Krasheninnikov, A. V.; Puska, M. Electronic stopping power from first-principles calculations with account for core electron excitations and projectile ionization. *Phys. Rev. B: Condens. Matter Mater. Phys.* **2014**, *89*, 035120.
(64) Zhao, S.; Kang, W.; Xue, J.; Zhang, X.; Zhang, P. Comparison of electronic energy loss in graphene and BN sheet by means of time-dependent density functional theory. *J. Phys.: Condens. Matter* **2015**, *27*, 025401.
(65) Gruber, E.; Wilhelm, R. A.; Petuya, R.; Smejkal, V.; Kozubek, R.; Hierzenberger, A.; Bayer, B. C.; Aldazabal, I.; Kazansky, A. K.; Libisch, F.; Krasheninnikov, A. V.; Schleberger, M.; Facsko, S.; Borisov, A. G.; Arnau, A.; Aumayr, F. Ultrafast electronic response of graphene to a strong and localized electric field. *Nat. Commun.* **2016**, *7*, 13948.
(66) Vázquez, H.; Kononov, A.; Kyritsakis, A.; Medvedev, N.; Schleife, A.; Djurabekova, F. Electron cascades and secondary electron emission in graphene under energetic ion irradiation. 2020, 2011.15117, arXiv. http://arxiv.org/abs/2011.15117 (accessed April 5, 2021).
(67) He, W.; Chen, C.; Xu, Z. Electronic excitation in graphene under single-particle irradiation. *Nanotechnology* **2021**, *32*, 165702.
(68) Ziegler, J. F.; Ziegler, M. D.; Biersack, J. P. SRIM − The stopping and range of ions in matter (2010). *Nucl. Instrum. Methods Phys. Res., Sect. B* **2010**, *268*, 1818−1823.
(69) Figueroa, E. A.; Cantero, E. D.; Eckardt, J. C.; Lantschner, G. H.; Valdés, J. E.; Arista, N. R. Threshold effect in the energy loss of slow protons and deuterons channeled in Au crystals. *Phys. Rev. A: At., Mol., Opt. Phys.* **2007**, *75*, 010901.
(70) Cantero, E. D.; Lantschner, G. H.; Eckardt, J. C.; Arista, N. R. Velocity dependence of the energy loss of very slow proton and deuteron beams in Cu and Ag. *Phys. Rev. A: At., Mol., Opt. Phys.* **2009**, *80*, 032904.
(71) Markin, S. N.; Primetzhofer, D.; Spitz, M.; Bauer, P. Electronic stopping of low-energy H and He in Cu and Au investigated by time-of-flight low-energy ion scattering. *Phys. Rev. B: Condens. Matter Mater. Phys.* **2009**, *80*, 205105.
(72) Ward, B. W.; Notte, J. A.; Economou, N. P. Helium ion microscope: A new tool for nanoscale microscopy and metrology. *J. Vac. Sci. Technol. B* **2006**, *24*, 2871−2874.
(73) Notte, J; Hill, R; McVey, S; Farkas, L; Percival, R; Ward, B An Introduction to the Helium Ion Microscope. *Microsc. Microanal.* **2006**, *12*, 126.
(74) Hlawacek, G.; Veligura, V.; van Gastel, R.; Poelsema, B. Helium ion microscopy. *J. Vac. Sci. Technol., B: Nanotechnol. Microelectron.: Mater., Process., Meas., Phenom.* **2014**, *32*, 020801.
(75) Correa, A. A. Calculating electronic stopping power in materials from first principles. *Comput. Mater. Sci.* **2018**, *150*, 291−303.
(76) Lakits, G.; Aumayr, F.; Heim, M.; Winter, H. Threshold of ion-induced kinetic electron emission from a clean metal surface. *Phys. Rev. A: At., Mol., Opt. Phys.* **1990**, *42*, 5780−5783.
(77) Runge, E.; Gross, E. K. U. Density-Functional Theory for Time-Dependent Systems. *Phys. Rev. Lett.* **1984**, *52*, 997−1000.
(78) Marques, M.; Gross, E. Time-dependent density functional theory. *Annu. Rev. Phys. Chem.* **2004**, *55*, 427−455.
(79) Marques, M. *Time-Dependent Density Functional Theory*; Springer Science & Business Media, 2006.
(80) Ullrich, C. A. *Time-Dependent Density-Functional Theory: Concepts and Applications*; Oxford University Press, 2012.
(81) Ullrich, C. A.; Yang, Z.-h. A brief compendium of time-dependent density-functional theory. *Braz. J. Phys.* **2014**, *44*, 154−188.
(82) Gygi, F. Architecture of Qbox: A scalable first-principles molecular dynamics code. *IBM J. Res. Dev.* **2008**, *52*, 137−144.
(83) Schleife, A.; Draeger, E. W.; Kanai, Y.; Correa, A. A. Plane-wave pseudopotential implementation of explicit integrators for time-dependent Kohn-Sham equations in large-scale simulations. *J. Chem. Phys.* **2012**, *137*, 22A546.
(84) Schleife, A.; Draeger, E. W.; Anisimov, V.; Correa, A. A.; Kanai, Y. Quantum Dynamics Simulation of Electrons in Materials on High-Performance Computers. *Comput. Sci. Eng.* **2014**, *16*, 54−60.
(85) Draeger, E. W.; Andrade, X.; Gunnels, J. A.; Bhatele, A.; Schleife, A.; Correa, A. A. Massively parallel first-principles simulation of electron dynamics in materials. *J. Parallel Distr. Com.* **2017**, *106*, 205−214.
(86) Draeger, E. W.; Gygi, F. Qbox code, Qb@ll version. 2018; https://github.com/LLNL/qball, Lawrence Livermore National Laboratory (accessed May 12, 2021).
(87) Dreizler, R. M.; Gross, E. K. U. *Density Functional Theory: an Approach to the Quantum Many-Body Problem*; Springer-Verlag, 1990.
(88) Zangwill, A.; Soven, P. Resonant Photoemission in Barium and Cerium. *Phys. Rev. Lett.* **1980**, *45*, 204−207.
(89) Zangwill, A.; Soven, P. Resonant two-electron excitation in copper. *Phys. Rev. B: Condens. Matter Mater. Phys.* **1981**, *24*, 4121−4127.
(90) Vanderbilt, D. Optimally smooth norm-conserving pseudopotentials. *Phys. Rev. B: Condens. Matter Mater. Phys.* **1985**, *32*, 8412−8415.
(91) Kresse, G.; Furthmüller, J. Efficient iterative schemes for ab initio total-energy calculations using a plane-wave basis set. *Phys. Rev. B: Condens. Matter Mater. Phys.* **1996**, *54*, 11169−11186.
(92) Kresse, G.; Joubert, D. From ultrasoft pseudopotentials to the projector augmented-wave method. *Phys. Rev. B: Condens. Matter Mater. Phys.* **1999**, *59*, 1758−1775.
(93) Monkhorst, H. J.; Pack, J. D. Special points for Brillouin-zone integrations. *Phys. Rev. B* **1976**, *13*, 5188−5192.
(94) Trickey, S. B.; Müller-Plathe, F.; Diercksen, G. H. F.; Boettger, J. C. Interplanar binding and lattice relaxation in a graphite dilayer. *Phys. Rev. B: Condens. Matter Mater. Phys.* **1992**, *45*, 4460−4468.
(95) Ooi, N.; Rairkar, A.; Adams, J. B. Density functional study of graphite bulk and surface properties. *Carbon* **2006**, *44*, 231−242.
(96) Klintenberg, M.; Lebègue, S.; Ortiz, C.; Sanyal, B.; Fransson, J.; Eriksson, O. Evolving properties of two-dimensional materials: from graphene to graphite. *J. Phys.: Condens. Matter* **2009**, *21*, 335502.
(97) Castro, A.; Marques, M. A. L.; Rubio, A. Propagators for the time-dependent Kohn-Sham equations. *J. Chem. Phys.* **2004**, *121*, 3425−3433.
(98) Kang, K.; Kononov, A.; Lee, C.-W.; Leveillee, J. A.; Shapera, E. P.; Zhang, X.; Schleife, A. Pushing the frontiers of modeling excited electronic states and dynamics to accelerate materials engineering and design. *Comput. Mater. Sci.* **2019**, *160*, 207−216.
(99) Rickhaus, P.; Liu, M.-H.; Kurpas, M.; Kurzmann, A.; Lee, Y.; Overweg, H.; Eich, M.; Pisoni, R.; Taniguchi, T.; Watanabe, K.; Richter, K.; Ensslin, K.; Ihn, T. The electronic thickness of graphene. *Science Advances* **2020**, *6*, eaay8409.
(100) Blaiszik, B.; Chard, K.; Pruyne, J.; Ananthakrishnan, R.; Tuecke, S.; Foster, I. The Materials Data Facility: Data services to advance materials science research. *JOM* **2016**, *68*, 2045−2052.
(101) Kononov, A.; Schleife, A. Dataset for "Anomalous stopping and charge transfer in proton-irradiated graphene". 2021; https://www.doi.org/10.18126/xnxt-wn6i (accessed May 12, 2021).

https://doi.org/10.1021/acs.nanolett.1c01416
Nano Lett. 2021, 21, 4816−4822